A universal transition to turbulence in channel flow

Masaki Sano[*] and Keiichi Tamai

Department of Physics, The University of Tokyo

7-3-1 Hongo, Bunkyo-ku, Tokyo 113-0033

Details of Image analysis

To obtain a background profile, the spatial profile of the scattered light intensity for the laminar state, $R(x,z,t)$, was captured at $Re \sim 600$ as movies for 100 sec every day before and after the series of measurements of turbulence. Then time average of the background $R_0(x,z) = \langle R(x,z,t) \rangle_t$ at each pixel was calculated presuming that the spatial resolution is sufficient. (1 pixel size in the image corresponds to $\sim$1.25 mm ($=h/2$) on the surface of the channel.) After taking movies for each Re number, each frame of the movie was normalized by dividing by the background to reduce inhomogeneity due to the illumination, *i.e.*, a normalized image $N(x,z,t)$ was calculated as $N(x,z,t) \equiv I(x,z,t)/R_0(x,z)$, where $I(x,z,t)$ is the original image and $R_0(x,z)$ is the background image. (Figures S2a, S2b and S2c show examples of the original image, $I(x,z,t)$, the background image $R_0(x,z)$, and the normalized image $N(x,z,t)$, respectively as a snapshot.) Then $N(x,z,t)$ is multiplied and shifted by certain numbers in order to save the memory storage. The standard deviation $\sigma(x,z)$ of the intensity fluctuations for the laminar state, $R(x,z,t)/R_0(x,z)$ was calculated. (Figure S3 shows the probability distribution function (PDF) of intensity fluctuations of a laminar state and PDF of the flow with turbulent spots embedded in a laminar state.) Turbulent spots were detected by the following procedure: Time series of the image intensity measured at each pixel point, $N(x,z,t)$, are created by fixing x and z. If the intensity deviated from expected values of the laminar state more than $\pm n \times \sigma(x,z)$ ($n = 3$ is used in most cases), space-time point (x,z,t) is regarded as a turbulent state, otherwise regarded as a laminar state. After assigning turbulent (active) or laminar (inactive) state for all x, z, and t, the cluster sizes of the spatially connected turbulent regions were calculated at each time instance. Clusters whose sizes were larger than h^2 were regarded as turbulent regions and the remaining small clusters as laminar regions, by assuming that the minimum size for localized turbulent eddies at moderate Re cannot be smaller than h. A typical result of the binarization is shown in Fig. S2d.

Supplementary Note

This supplementary note demonstrates the influence of an advection and an active boundary condition on systems exhibiting the transition which falls onto the directed percolation universality class (DP) by a numerical simulation on a simple model.

The model we consider is similar to the (1+1)-dimensional (*i.e.*, one-dimensional in space and one-dimensional in time, hereafter abbreviated as (1+1)D) directed bond percolation [1] model (which is known to exhibit a continuous transition belonging to DP), except the existence of the wall and asymmetry in connection in order to mimic the effect of advection (Fig. S4a). More formally, the model with a percolation probability p is defined on a set $s = \{s_i\}_{i=0}^{N-1}$ of a local binary variable s_i (where i is the number of sites from the wall and N is the size of the system) by the following rules:

$$s_0(t) = 1 \text{ for } \forall t \qquad (1)$$

$$s_i(t+1) = \begin{cases} 1; & \text{if } (s_{i-1}(t)=1 \text{ and } z^- < p) \text{ or } (s_i(t)=1 \text{ and } z^0 < p) \\ 0; & \text{otherwise} \end{cases} \text{ for } i \geq 1 \qquad (2)$$

where $s_i = 0$ and $s_i = 1$ denote an inactive state and an active state respectively, and $z^-, z^0 \in (0,1)$ are randomly generated variables. Note that the critical percolation probability p_c of the model is expected to be identical to the one of ordinary directed bond percolation, which is very accurately estimated to be $p_c = 0.64470015(5)$ in past studies [2]. Typical dynamics of the model is shown in Fig. S4b. We can clearly see (especially for $p = 0.64245$ and $p = 0.64570$) that localized clusters of active sites are moving along the direction of the advection.

We performed a Monte—Carlo simulation on the lattice of the size $N = 8192$. We started our simulation with the system whose site in the wall is active and other sites are inactive. Each Monte—Carlo step consists of a parallel update of each site based on the rule (1) and (2). Here we perform a stationary simulation: We first run the simulation for 15×10^4 steps (which is about 20 times longer than the steps needed for an active state generated on the wall to reach the other end of the lattice) and then the statistics are accumulated over another 85×10^4 steps. The simulation is repeated over 16 times to improve statistics.

We first measured the order parameter ρ as a function of the distance x from the wall. The order parameter $\rho(x)$ is defined as a probability that the x th site from the wall is active during the stationary simulation. Figure S5a shows that $\rho(x)$ decays exponentially when the percolation probability p is smaller than the critical value p_c, while it saturates to a finite value when $p > p_c$. This behavior allows us to define a decay length L as a characteristic length of the exponential decay at $p < p_c$, i.e.,

$\rho(x) \sim \exp(-x/L)$ for sufficiently large x. As shown in Fig. S5b, we find that L as a function of $p_c - p$ shows a power-law behavior in a vicinity of the critical point. Fitting by a function $L \sim (p_c - p)^{\nu_1}$ yields $\nu_1 = 1.71(5)$, which is close to the theoretical value of $\nu_{\parallel}$ for (1+1)D DP: $\nu_{\parallel}^{DP} = 1.733847(1)$ (Note that, as usual for a finite system, deviation from the power-law behavior is observed at the point where the resulting L is comparable to N; then a finite- size effect is no longer negligible). These results are consistent with those reported by Costa *et al.* [3], who studied asymmetric contact process (which is also known to belong to the DP universality class [4]) driven by an active boundary condition. We also measured the order parameter ρ at the fixed observation point (8,000$^{\text{th}}$ site from the active wall) for various value of p. As expected, a power-law behavior $\rho(p) \sim (p - p_c)^{\beta}$ is observed for $p \geq 0.64570$ (Fig. S5c). We obtain the critical exponent β as a best fit $\beta = 0.271(8)$, which is in a very good agreement with (1+1)D DP $\beta = 0.276486(8)$, although a deviation from the power law is present for $\varepsilon \sim 10^{-3}$ as expected.

Next, we measured a distribution of durations τ of an inactive state for a fixed observation point, as done in the experiment discussed in a main text. We made a histogram for τ, and then calculated a complementary cumulative probability distribution $P(\tau)$: $P(\tau) = 1 - \sum_{t=1}^{\tau} N(t) - \sum_{t=1}^{T} N(t)$, where T is a Monte—Carlo steps for each realization. We confirmed that the distribution $P(\tau)$ as a function of τ converged as long as we measured $P(\tau)$ at the site sufficiently far from the wall for $p > p_c$. The distribution $P(\tau)$ is measured at a fixed point ($x = 5000$) for various values of $p(> p_c)$ and the results are shown in Fig. S6a, where we can clearly see an exponential decay $P(\tau) \sim \exp(-\tau/\xi)$ for a sufficiently large τ. The characteristic length ξ of the decay turned out to obey a power law $\xi \sim (p - p_c)^{-\nu_2}$, whose exponent is significantly different from the exponent $\nu_{\parallel}$ associated with a correlation time but very close to the exponent $\nu_{\perp}$ associated with a correlation length (Fig. S6b). As discussed in the main text, this behavior can be understood by comparing the growth of the correlation length and correlation time. In systems exhibiting the DP universality, the correlation time grows much faster than the correlation length (recall $\nu_{\parallel} > \nu_{\perp}$), and therefore the clusters of the active state become thinner and thinner as we approach the critical point (as we can see in Fig. S4b). Thus, by fixing the observation point and measuring the duration of the inactive state, we are actually probing the spatial distance between the clusters, which is expected to correspond to the spatial correlation length.

We now explore the universal scaling hypothesis of the inactive interval distribution. The discussion in the previous paragraph implies the inactive interval distribution probes spatial interval between the active clusters, so we postulate that the inactive interval distribution has scaling properties analogous to that of spatial two-point correlation function. That is, we assume that under the transformation of the control parameter $\varepsilon \mapsto \lambda\varepsilon$ and interval $\tau \mapsto \lambda^{-\nu_\perp}\tau$, the inactive interval distribution also scales as $N \mapsto \lambda^\eta N$ with some suitable exponent η:

$$N(\tau) \sim \lambda^{-\eta} f(\lambda^{-\nu_\perp}\tau, \lambda\varepsilon) \tag{3}$$

although the inactive interval distribution is significantly different from an ordinary two-point correlation function as pointed out by Hinrichsen [5]. Accepting the postulation and choosing the scaling parameter $\lambda = \tau^{1/\nu_\perp}$, simple scaling argument leads us to $\eta = 2\nu_\perp - \beta$ and to the following scaling hypothesis [5]:

$$N(\tau) \sim \tau^{-\mu_\perp} f(\varepsilon^{\nu_\perp}\tau) \text{ where } \mu_\perp = 2 - \beta/\nu_\perp \tag{4}$$

This hypothesis first implies $N(\tau) \sim \tau^{-\mu_\perp}$ in a vicinity of the critical point ($\varepsilon \to 0$). Indeed, as shown in Fig. S7a, we observe a power-law decay of the distribution function, and the estimated exponent 1.74(2) is close to $\mu_\parallel^{DP} = 1.747928(7)$ derived from the above scaling relation and the theoretical value of β and $\nu_\perp$ for (1+1)-dimensional DP. Also, integrating the hypothesis (4) from τ to ∞, and with a suitable normalization, we obtain the scaling hypothesis for $P(\tau)$:

$$P(\tau) = \frac{\int_\tau^\infty dt N(t)}{\int_0^\infty dt N(t)} \sim \varepsilon^{\nu_\perp(\mu_\perp - 1)} g(\varepsilon^{\nu_\perp}t) \text{ where } g(x) = \int_x^\infty dx' x'^{-\mu_\perp} f(x'). \tag{5}$$

We rescale $P(\tau)$ according to the scaling hypothesis (5), and we observe a clear collapse onto a single, universal function as presented in Fig. S7b. Thus, we numerically confirmed that the scaling hypotheses (4) and (5) indeed hold in this case (although it may be slightly modified due to some intermittency effects [6]).

We conclude that, in a system with advection and an active boundary, one can experimentally estimate all three critical exponents β, $\nu_\parallel$ and $\nu_\perp$ by measuring an order parameter at a point sufficiently far from the boundary, spatial dependence of the order parameter, and distribution of durations of an inactive state, respectively. Note that the exponent $\mu_\perp$, which is related to β and $\nu_\perp$ by equation (4), can be estimated from the distribution of durations of an inactive state as well.

As an auxiliary information, we briefly report simulation results on (2+1)D simulation. For (2+1)D simulation, our model (with an active wall and advection) is based on a directed bond percolation model in a body-centered-cubic lattice, whose critical

percolation probability p_c has been recently reported to be $p_c = 0.28733837(2)$ [8]. We performed Monte—Carlo simulation in a system with 1,024 sites in streamwise direction and 128 sites in spanwise direction. In this simulation, statistics are accumulated over 40×10^4 steps after a warmup of 5×10^4 steps. The results presented in Fig. S8 and Fig. S9 indicate that one can also obtain consistent results by a numerical simulation on (2+1)D variant of this model, with moderate system size and statistics.

Supplementary Figures
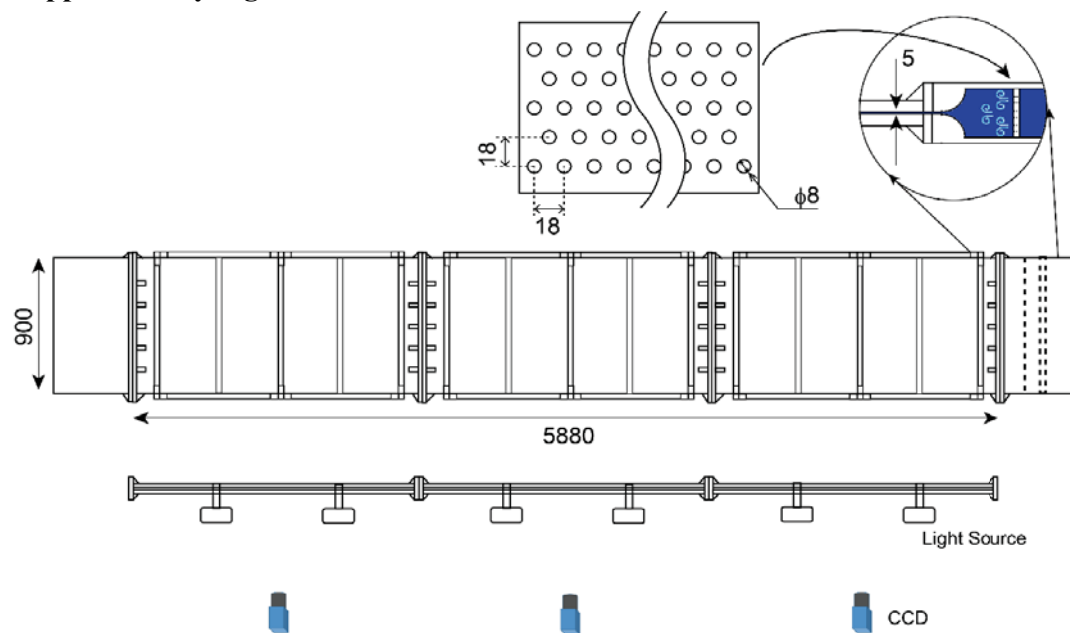
Figure S1. Experimental apparatus.
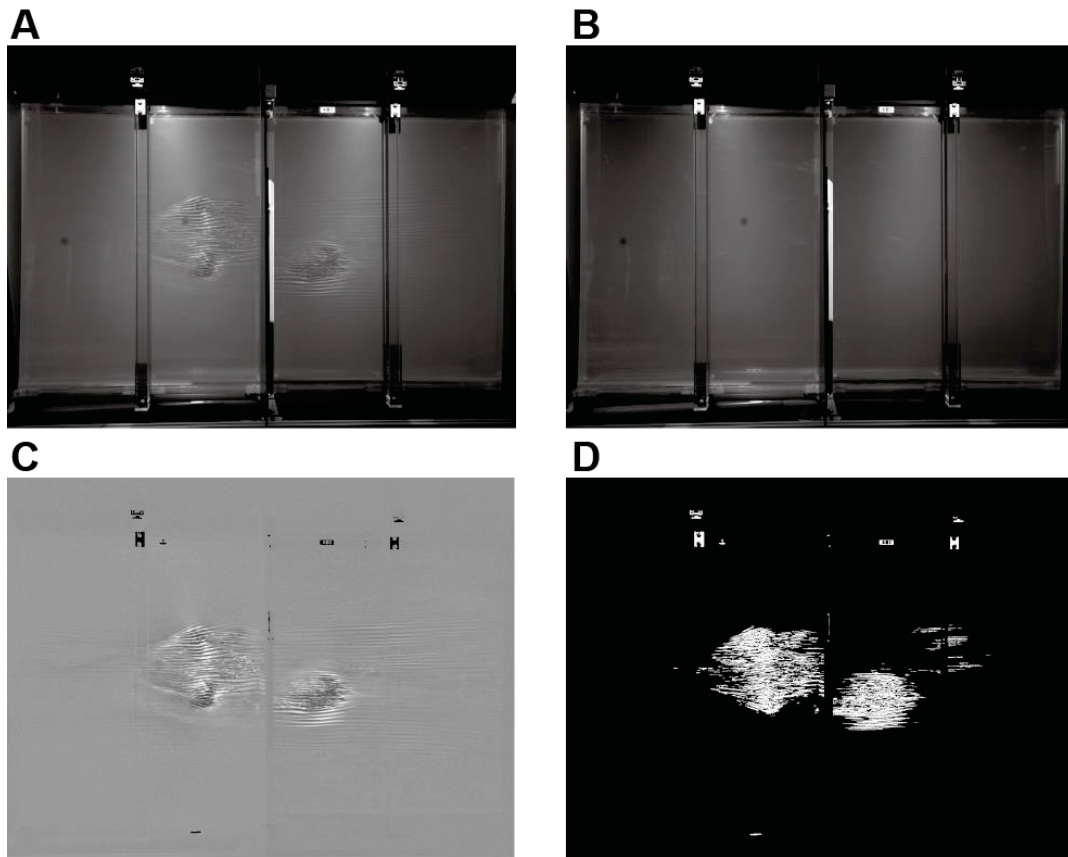
Figure S2. Examples of image processing. a, Original image (6 illuminating projectors are used in this sample.). **b**, Background image taken at *Re*~600 and averaged in time. **c**, Normalized image divided by the background image. **d**, Binary image showing detected turbulent regions which exceed more than 3σ(*x*,*z*) at each pixel.
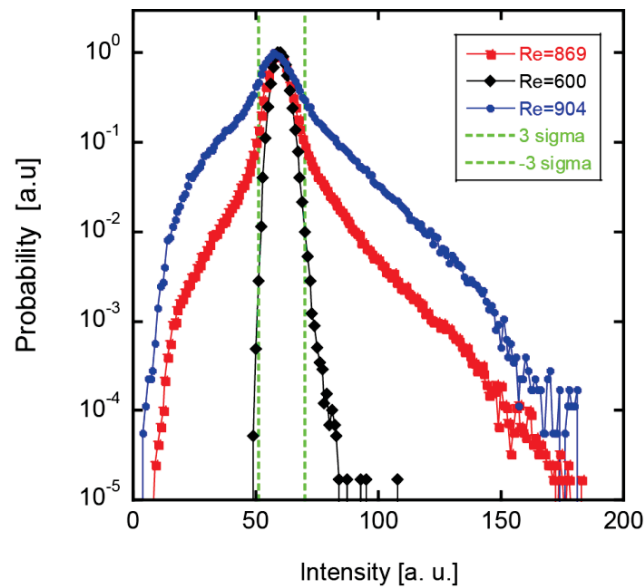
Figure S3. Typical behavior of image intensity fluctuations. Typical probability distribution functions (PDF) of image intensity fluctuations measured at a fixed location ($x\sim3.2$m) in a small region (25 mm $\times$ 25mm) and accumulated for 1000 frames. All movies were normalized by a time averaged background image taken for a laminar state ($Re\sim600$), then histogram was accumulated for the normalized images. Black symbol represents PDF of intensity fluctuations in a laminar state ($Re\sim600$, ♦). PDF is close to a Gaussian distribution. As Re increases to $Re=869$ (■) and $Re=904$ (●), the turbulent spots gradually increase. Accordingly, intensity fluctuations show large deviations from the Gaussian both to brighter and darker sides. Note that PDF is a superposition of a narrow Gaussian originated from laminar states and a broad distribution with large skewed wings originated from turbulent spots. Large deviations which exceed $\pm3\times\sigma(x,z)$ (green dashed line) from the mean laminar intensity were regarded as the turbulent state.
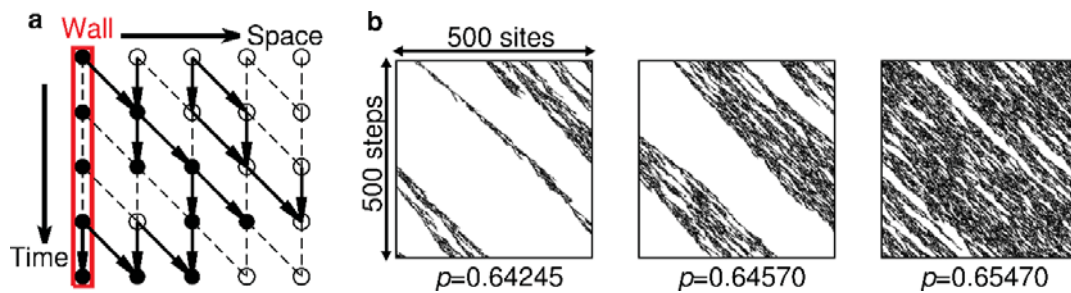
Figure S4. Schematic picture of the (1+1)D directed bond percolation model with active wall and asymmetric connection. a, Each site (circle) has two states, namely an active state (black) and an inactive state (white). Each bond between the sites is open (solid arrow) with probability p, or otherwise closed (dashed line). Sites in an "active wall" (the leftmost) are forced to be active, and sites connected with an active sites are also active. See text for a more formal definition of the model. **b**, Typical spatiotemporal dynamics observed at the 5,000—5,500 sites away from the active wall. When p is smaller than the critical value ($p = 0.64245$), the clusters of active states tend to die out. When p is near the critical point ($p = 0.64570$), clusters of active sites are still localized in space, but it can be sustained. When p is much larger than the critical value ($p = 0.65470$), the cluster of the active sites dominate the entire space.
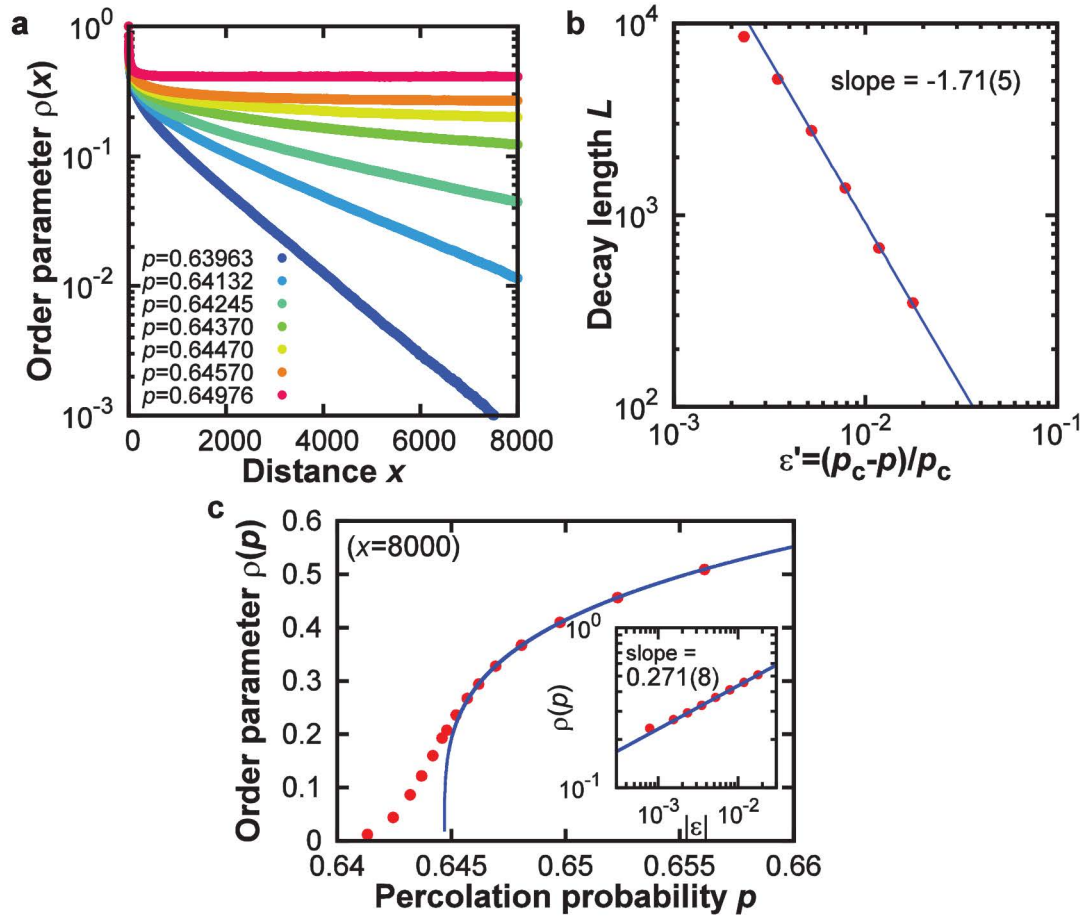
Figure S5. Measurement of the Order parameter in (1+1)D numerical simulation. a, Behavior of the order parameter $\rho(x)$ with respect to the distance x from the active wall. When the percolation probability p is significantly smaller than p_c, exponential decay $\rho(x) \sim \exp(-x/L)$ is observed (where L is a decay length), while a convergence to a finite value is observed when p is sufficiently larger than p_c. **b**, The decay length L as a function of $\varepsilon' = (p_c - p)/p_c$. The blue solid line is a best fit by a power law. Data with $\varepsilon' > 5 \times 10^{-3}$ are used for the fitting, and the error represents a 95% confidence interval in the sense of Student's t. **c**, Order parameter measured at 8,000th site from the active wall. Variation of the saturated value for $p > p_c$ is smaller than the symbol. The inset shows the same data in a logarithmic scale. A solid blue line shows the best fit (data with $\varepsilon \equiv (p - p_c)/p_c > 10^{-3}$ are used) by a power law, giving $\beta = 0.271(8)$. Number in the parentheses represent a 95% confidence interval in a sense of Student's t.
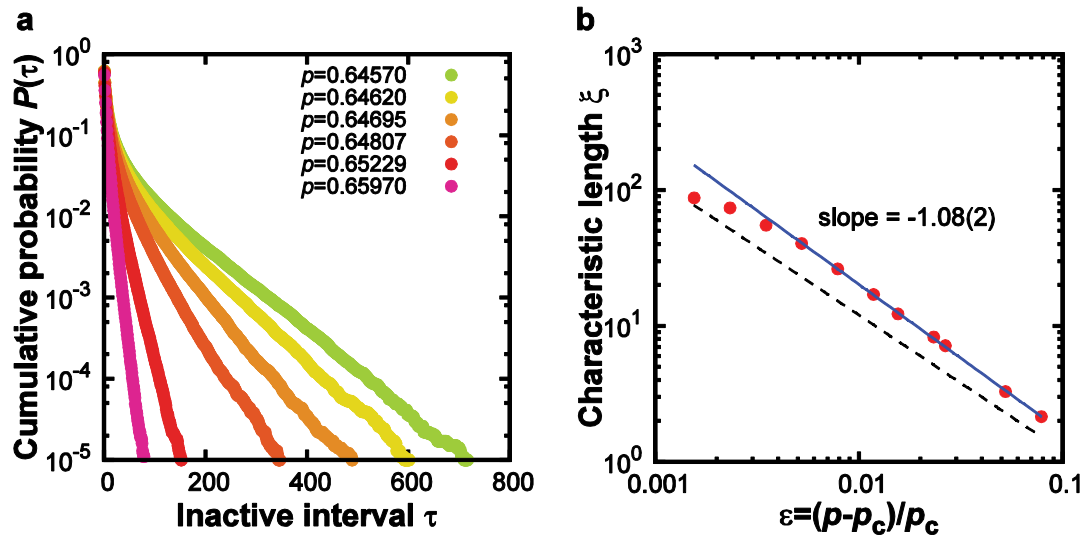
Figure S6. Measurement of the inactive interval distribution in (1+1)D numerical simulation. a, The probability distribution $P(\tau)$ that an inactive state is sustained up to τ steps is measured for various values of $p > p_c$, showing an exponential decay for a sufficiently large τ. **b,** The characteristic length ξ of the exponential decay of the distribution $P(\tau)$. Number in the parentheses represent a confidence interval in a sense of Student's *t*. Note that deviation from the power law in a vicinity of the critical point is observed if we measure the distribution at the point too near the active wall, where the steady state of the order parameter is not yet achieved. Similar situations occur in the experiment with turbulent liquid crystal [7] and with channel flow (see main text). Thus the data points with $\varepsilon < 0.003$ were removed for the fitting. The solid blue line is a best fit and the black dashed line is a guide to eye for $\xi \sim \varepsilon^{-1}$.
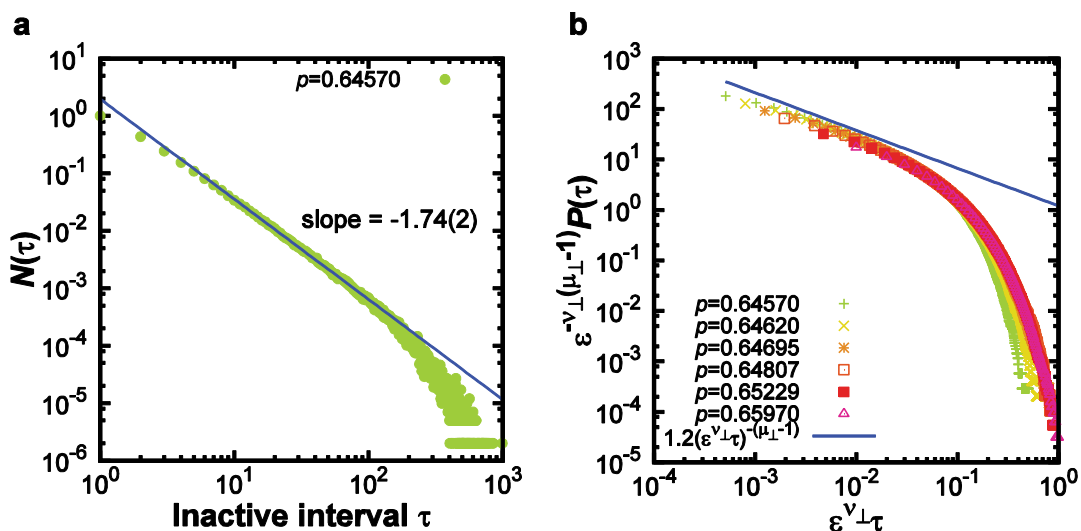
Figure S7. Scaling property of the inactive interval distribution in (1+1)D numerical simulation. a, The inactive interval distribution $N(\tau)$ normalized by $N(1)=1$ is shown in a logarithmic scale. Solid blue line shows the best fit, giving $\mu = 1.74(2)$. Number in the parentheses represent a confidence interval in a sense of Student's t. Here the data points with very large τ ($\tau \geq 100$) are removed for the fitting, because crossover from power-law decay to exponential one is observed, as also demonstrated in Fig. S6a. **b**, The complementary cumulative distribution function $P(\tau)$ is rescaled according to the scaling hypothesis (5) (see text). Although the theoretical value of $\nu_\perp$ and $\mu_\perp$ for (1+1)D DP is used in this scaling plot, a collapse of similar quality is obtained even if we use the value estimated by the simulation. Deviation from the universal scaling function in a vicinity of the critical point is due to a finite size effect, as also observed in the experiment. Solid blue line is guide to eye for $(\varepsilon^{\nu_\perp}\tau)^{-(\mu_\perp - 1)}$.
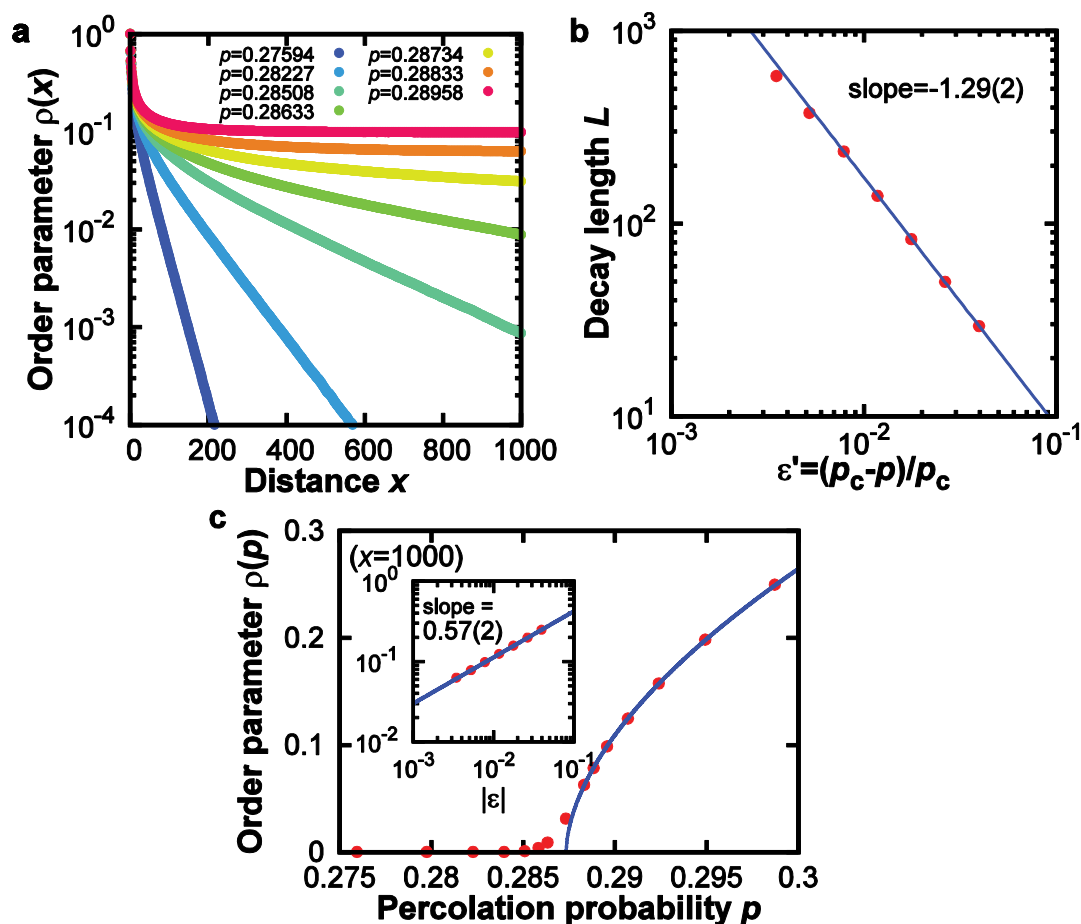
Figure S8. Measurement of the Order parameter in (2+1)D numerical simulation. a, Behavior of the order parameter $\rho(x)$ with respect to the distance x from the active wall. **b**, The decay length L as a function of $\varepsilon' = (p_c - p)/p_c$. Estimated value of $\nu_\parallel$ is in a good agreement with theoretical value of (2+1)D DP: $\nu_\parallel = 1.295(6)$. **c**, Order parameter measured at $1{,}000^{\text{th}}$ site from the active wall. The inset shows the same data in a logarithmic scale. Critical exponent β estimated from a power-law behavior is very close to (2+1)D DP: $\beta = 0.584(4)$. Data with $\varepsilon' > 5 \times 10^{-3}$ are used for the fitting, and the error represents a 95% confidence interval in the sense of Student's t.
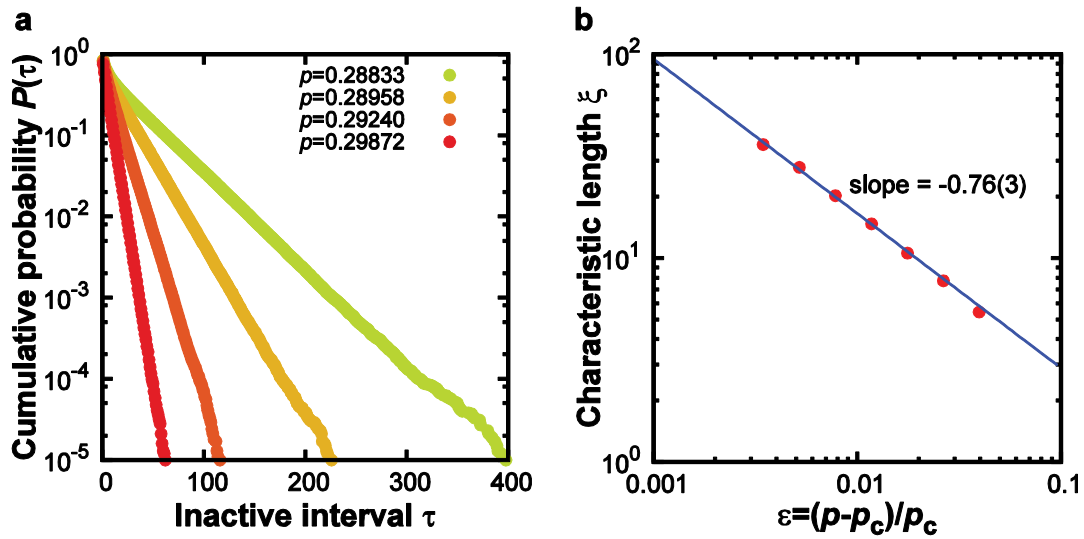
Figure S9. Measurement of the inactive interval distribution in (2+1)D numerical simulation. a, The probability distribution $P(\tau)$ that an inactive state is sustained up to τ steps is measured at a fixed point ($x = 800$) for various values of $p > p_c$, showing an exponential decay for a sufficiently large τ. **b**, The characteristic length ξ of the exponential decay of the distribution $P(\tau)$ as a function of $\varepsilon = (p - p_c)/p_c$. Estimated value of $\nu_\perp$ is in a good agreement with theoretical value of (2+1)D DP: $\nu_\perp = 0.734(4)$. Number in the parentheses represent a 95% confidence interval in a sense of Student's t.

References

[1] Essam, J. W., De'Bell, K., Adler, J. & Bhatti, F.M. Analysis of extended series for bond percolation on the directed square lattice. *Phys. Rev. B* **33**, 1982-1986 (1986).

[2] Jensen, I., Temporally Disordered Bond Percolation on the Directed Square Lattice. *Phys. Rev. Lett.* **75**, 4988-4991 (1996).

[3] Costa, A., Blythe, R.A. & Evans, M.R. Discontinuous transition in a boundary driven contact process. *J. Stat. Mech.* **2010**, P09008 (2010).

[4] Schonmann, R. H. The asymmetric contact process. *J. Stat. Phys.* **44**, 505-534 (1986).

[5] Henkel, M., Hinrichsen, H. & Lübeck, S. *Non-Equilibrium Phase Transitions Volume I: Absorbing Phase Transitions* (Springer, Dordrecht, 2008).

[6] Henkel, M. & Peschanski, R. Intermittency studies in directed bond percolation. *Nucl. Phys. B* **390**, 637-652 (1993).

[7] Takeuchi, K. A., Kuroda M., Chaté, H. & Sano, M. Experimental realization of directed percolation criticality in turbulent liquid crystals. *Phys. Rev. E* **80**, 051116 (2009).

[8] Wang, J., Zhou, Z., Liu, Q., Garoni, T. M. & Deng, Y. High-precision Monte Carlo study of directed percolation in $(d+1)$ dimensions. *Phys. Rev. E* **88**, 042102 (2013).